Remote Sensing of Environment 231 (2019) 111276

Contents lists available at ScienceDirect

Remote Sensing of Environment

journal homepage: www.elsevier.com/locate/rse

# Derivation of canopy light absorption coefficient from reflectance spectra

Anatoly Gitelson[a,b,*], Andrés Viña[c,d], Alexei Solovchenko[e,f,g], Timothy Arkebauer[h], Yoshio Inoue[i,j]

[a] School of Natural Resources, University of Nebraska-Lincoln, Lincoln, NE 68583, USA
[b] Israel Institute of Technology (Technion), Haifa 3200003, Israel
[c] Center for Systems Integration and Sustainability, Department of Fisheries and Wildlife, Michigan State University, Lansing, MI 48823, USA
[d] Geography Department, University of North Carolina, Chapel Hill, NC 27599, USA
[e] Departament of Bioengineering, Faculty of Biology, Lomonosov Moscow State University, Moscow, Russia
[f] Michurin Federal Scientific Centre, Michurinsk, Russia
[g] Peoples Friendship University of Russia (RUDN University), Moscow, Russia
[h] Department of Agronomy and Horticulture, University of Nebraska-Lincoln, Lincoln, NE 68583, USA
[i] Research Center for Advanced Science and Technology, University of Tokyo, Tokyo 153-8904, Japan
[j] Institute for Agro-Environmental Sciences, NARO (NIAES), Tsukuba 305-8604, Japan

ARTICLE INFO

Edited by Jing M. Chen

*Keywords:*
Absorption and scattering coefficients
Plant canopy
Pigment content

ABSTRACT

The light absorption coefficient of vegetation is related to the content and composition of pigments in the plant canopy. It is a useful metric for understanding the spatial and temporal dynamics of the absorbed solar radiation, photosynthetic capacity, and productivity of vegetation. Still, its estimation in vivo is challenging due to the large variability induced by numerous features: canopy-related factors, including biochemical and structural characteristics, and factors external to the canopy such as soil background, solar irradiation, and sun-target-sensor geometry conditions. Here we revisit a semi-analytical modeling framework for deriving the light absorption coefficient of plant canopies from reflectance data. The proposed approach is based on the partition of the total light absorption coefficient into photosynthetic and non-photosynthetic pigment components in the canopy, and canopy backscattering. The model-derived absorption coefficient of chlorophyll was compared with field matchups of total canopy chlorophyll content in three crops with contrasting leaf structures, canopy architectures and photosynthetic pathways: maize, soybean, and rice. The model allows for the derivation of absorption coefficient spectra across the photosynthetically active radiation and the red edge spectral regions, as well as accurate estimations of canopy chlorophyll content, both of which are necessary for analyzing the physiological and phenological status, and the canopy-level photosynthetic capacity, of plants.

## 1. Introduction

Chlorophyll, Chl, is a magnesium-tetrapyrrole molecule, the main determinant of the amount of solar radiation absorbed by plants, central to its conversion into chemical energy (Chen, 2014). In terrestrial plants there are two forms of this pigment, Chl *a* and Chl *b*, with slightly different chemical structures. These small differences cause variations in their absorption spectra (Chen, 2014) and in their functional properties [e.g., the most abundant Chl *a* is the primary pigment responsible for light-harvesting and photochemistry, while Chl *b* acts as an accessory light-harvesting pigment (Croce and Van Amerongen, 2014)]. While their relative concentrations vary in response to changes in environmental conditions (Richardson et al., 2002), for many applications estimation of the sum of Chl ($a + b$) is sufficient.

The importance of total foliar Chl content, [Chl], for terrestrial carbon dynamics (Gamon et al., 1995; Gitelson et al., 2016; Gitelson et al., 2006b; Peng et al., 2011; Wu et al., 2009) and their cascading consequences on ecosystem processes (Joiner et al., 2014; Li et al., 2018; Piao et al., 2005; Xia et al., 2015; Youngentob et al., 2015) and climate feedbacks (Fahey et al., 2017; Friend, 2010; Sippel et al., 2018) is well-established. Thus, information on the spatial and temporal dynamics of [Chl] is crucial for assessing not only biochemical and

*Abbreviations:* Chl, chlorophyll; NIR, near infra-red; RE, red edge; RMSE, root mean square error; NRMSE, normalized root mean square error; PAR, photosynthetically active radiation; APAR, absorbed PAR; LUE, light use efficiency; GPP, gross primary productivity; MTCI, MERIS terrestrial chlorophyll index; LAI, leaf area index

* Corresponding author at: School of Natural Resources, University of Nebraska-Lincoln, Lincoln, NE 68583, USA.
*E-mail address:* agitelson2@unl.edu (A. Gitelson).

https://doi.org/10.1016/j.rse.2019.111276
Received 21 February 2019; Received in revised form 13 June 2019; Accepted 22 June 2019

structural but also functional traits of vegetation (Gitelson et al., 2005; Luo et al., 2018; Ustin and Gamon, 2010) and their effects on human activities (Burke and Lobell, 2017; Deines et al., 2017).

Hundreds of papers have been published demonstrating the suitability of using imaging remote sensors for the synoptic assessment of the spatiotemporal dynamics of [Chl]. Yet, despite several technological advances, including the development of sophisticated optical imaging systems (e.g., Asner et al., 2015; Drusch et al., 2012; Frankenberg et al., 2014; Guanter et al., 2012) and analytical techniques (e.g., Blackburn, 2006; Dash and Curran, 2007; Gholizadeh et al., 2015; Inoue et al., 2016; Sun et al., 2018), much of the synoptic information on [Chl] dynamics is obtained using procedures whose effectiveness and accuracy are constrained to particular geographic locations, individual species, or species assemblages (Houborg et al., 2015; Yu et al., 2014; Zou et al., 2015). Notwithstanding the enormous published literature on the use of remote sensing techniques for assessing [Chl] dynamics, much more work is still needed to develop generic algorithms applicable to multiple, if not all, vegetation types, physiological pathways, health status, phenological phases, and environmental conditions. This requires an operational understanding of the absorption coefficient of Chl across these different conditions in the entire photosynthetically active radiation (PAR) spectral region (400–700 nm).

The absorption coefficient of vegetation is a metric used for determining how deep incident radiation in a particular wavelength penetrates the plant canopy before being absorbed. Thus, it is related to the pigment content and composition of the plants constituting the canopy. While information on the absorption coefficient of pigments (e.g., Chl) at canopy scales is necessary for understanding the spatial and temporal dynamics of absorbed radiation, photosynthetic capacity and vegetation productivity across broad geographic regions, its acquisition in vivo is challenging.

Although absorption coefficient relates to reflectance of vegetation, finding the relationship with reflectance at canopy scales is difficult, given that they are influenced by numerous factors: canopy-related including biochemical (e.g. leaf pigment content and composition) and structural (e.g. leaf structure, leaf area index, leaf angle distribution) traits, and external factors such as reflectance of the soil background, solar irradiance and sun-target-sensor geometry conditions. Thus, it is important that the absorption coefficient retrieved from reflectance should be minimally influenced by factors other than the pigment of interest. To this effect, three questions arise: (1) Is it possible to derive the canopy absorption spectra from canopy reflectance? (2) What is the relationship between reflectance and canopy absorption coefficient? And (3) Does the relationship between reflectance and absorption coefficient remain close across the entire PAR spectral range?

We have previously developed robust and accurate algorithms based on reflectance spectra for the remote assessment of pigment contents (Chl, carotenoids and anthocyanins) at leaf and canopy scales (Gitelson and Solovchenko, 2017; Gitelson et al., 2006a; Gitelson et al., 2005; Peng et al., 2017). These approaches are based on pigment content retrieved from pigment-specific reflectance spectral bands. The algorithms provided a practical and accurate way for assessing vegetation productivity through time and across different species, functional types, and broad geographic regions (Gitelson et al., 2016; Gitelson et al., 2008; Peng et al., 2011). Yet, to fully understand the foundations of the generality of these approaches, one needs first of all to *evaluate their capacity for deriving the absorption coefficient of pigments in different optical media across the entire PAR spectral region*. Here we evaluate the capacity for isolating a pigment absorption coefficient, namely the absorption coefficient of Chl, in the PAR region among different plant species with contrasting leaf structures, canopy architectures, and disparate photosynthetic physiology.

## 2. Conceptual framework

### 2.1. Basis for using reciprocal reflectance as a proxy of pigment absorption coefficient

In Kubelka-Munk theory (Kubelka and Munk, 1931), only two constants were introduced, the absorption coefficient (α) and the scattering coefficient (β), by means of which the ratio α/β of a layer of infinite thickness may be expressed. This ratio (called the remission function or the Kubelka-Munk function) is a function of the infinite reflectance ($\rho_{inf}$) of a layer in which further increase in thickness results in non-noticeable differences in reflectance (Kortum, 1969; Wendlandt and Hecht, 1966), expressed as.

$$f(\rho_{inf}) = (1-\rho_{inf})^2/2\rho_{inf} = \alpha/\beta \quad (1)$$

Importantly, $f(\rho_{inf})$ depends exclusively on the ratio α/β "but not on the absolute numerical values of these constants" as Kubelka and Munk underlined in their original paper (Kubelka and Munk, 1931), see also (Kortum, 1969). More recently a revision of the Kubelka–Munk theory was suggested by taking into account the effect of scattering on the path length of light propagation. It was shown that for some specific cases the Kubelka–Munk absorption and scattering coefficients may be non-linearly related to inherent absorption and scattering coefficients (Yang and Kruse, 2004). However, here we assume that the ratio of α to β does relate to the remission function, as described in Eq. (1).

While the remission function is based on a hypothetical optically thick layer in which further increases in thickness do not lead to an increase in $\rho_{inf}$, a vegetation canopy has limited optical depth, thus its reflectance may differ from $\rho_{inf}$. In terms of the Kubelka-Munk theory, the measured reflectance of a finite optical medium (such as a canopy) is defined as $\rho_0$, where the index 0 is used to designate an ideal black background. To find the relationship between canopy reflectance, $\rho_0$, and the ratio of inherent optical properties, α/β, one should first comprehend how close are $\rho_{inf}$ and $\rho_0$. The relationship between the measured reflectance $\rho_0$ and the reflectance of the infinite layer $\rho_{inf}$ may be retrieved from the equation (Kortum, 1969):

$$f(\rho_{inf}) = (1 + \rho_{inf}^2)/2\rho_{inf} = (1 + \rho_0^2 - T_0^2)/2\rho_0 - 1 \quad (2)$$

where $\rho_0$ and $T_0$ are the reflectance and transmittance of the medium, respectively.

Thus, in general, to find $f(\rho_{inf})$ for a vegetative canopy one needs to know both canopy reflectance and transmittance. However, canopy reflectance and transmittance depend on many biochemical and structural factors, while being also affected by irradiation conditions and the geometry (sun–viewer–object) of the measurement. Therefore, it is practically impossible to collect all the data required, especially canopy transmittance, as different hybrids and cultivars of even different plants of the same species often have very different canopy structures that change during the growing season. We attempted to simplify this challenge by inferring the relationship $\rho_{inf}$ vs. $\rho_0$ for leaves of different species in a wide range of [Chl] and then evaluating whether the corresponding findings at the leaf scale are applicable at canopy scales. This is essential since the measurements of reflectance and transmittance at the leaf level can be easily obtained using a radiometer connected to an integrating sphere, while those at canopy level are not so straightforward, particularly transmittance. At the canopy level such measurements may be carried out with upward- and downward-looking radiometers affixed with cosine diffusers and positioned at ground level and above the canopy, although they may not be reliably obtained at low to moderate vegetation fractions (Hanan et al., 2002). At the canopy level we used the results of transmittance and reflectance measurements of maize and soybean canopies with vegetation fractions above 70% (Viña, 2004).

At leaf scale, the numerator of Eq. (2), $(1 + \rho_0^2 - T_0^2)$, was close to unity (Fig. 1A) and $f(\rho_{inf})$ constitutes a hyperbolic function of $\rho_0$ – $f(\rho_{inf}) \propto (\rho_0)^{-1}$. For leaves with $\rho_0$ ranging from 0 to 50% ([Chl] ranging from

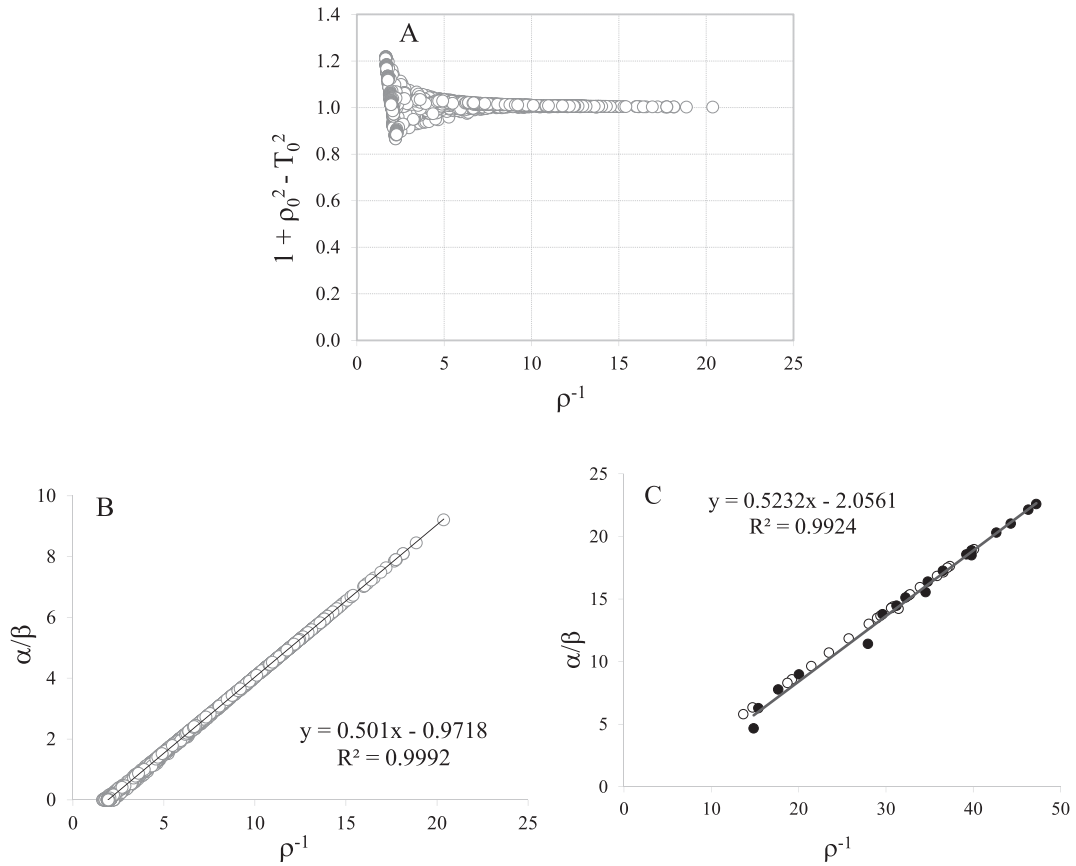


**Fig. 1.** (A) Numerator of Eq. (2), $(1 + \rho_0^2 - T_0^2)$, plotted versus reciprocal reflectance, $\rho_0^{-1}$, in leaves. (B and C) Ratio of absorption to scattering coefficient, $\alpha/\beta = f(\rho_{inf})$, plotted against reciprocal reflectance in (B) leaves (135 beech, chestnut, elm and maple leaves, and 150 soybean and maize leaves) and (C) canopy (maize and soybean) with vegetation fractions above 70%, modified from (Viña, 2004).

40 to 810 nmol/cm$^2$) and for canopies with vegetation fractions larger than 70%, the relationship between $f(\rho_{inf})$ and reciprocal reflectance, $\rho_0^{-1}$ was linear, with $R^2 > 0.99$ (Fig. 1B and C).

### 2.2. Isolation of canopy absorption coefficient

The close linear relationships between the Kubelka-Munk remission function and reciprocal reflectance found at both leaf and canopy scales (Fig. 1) laid a solid foundation for the retrieval of canopy absorption coefficient from reflectance spectra in the form:

$$(\rho_\lambda)^{-1} = (\alpha_{pigm} + \alpha_0)/\beta \quad (3)$$

where $(\rho_\lambda)^{-1}$ is canopy reciprocal reflectance, $\alpha_{pigm}$ is the absorption coefficient of the photosynthetic pigments in the canopy, $\alpha_0$ is the absorption coefficient of non-photosynthetic pigments, and $\beta$ is the scattering coefficient of the canopy. The canopy absorption coefficient determines the penetration depth of incident radiation in a particular wavelength before being absorbed, while the scattering coefficient determines the extinction rate of radiation as it traverses through a scattering medium. The former is governed mainly by leaf biochemistry (pigment content and composition) and influenced by leaf area index (LAI) and leaf angle distribution (LAD), while the latter is a function of canopy structural properties, including canopy density, LAI, LAD and leaf structure.

The reciprocal reflectance spectra of canopies (Fig. 2) exhibit two spectral regions with maximal $(\rho_\lambda)^{-1}$ values (in the blue, 400–500 nm, and the red, 650–700 nm). It is important to underline that $(\rho_\lambda)^{-1}$ in the green (500–580 nm) and red edge (around 700 nm) regions is quite high, reaching 45% of those in the red region (Fig. 2). This demonstrates a > 10-fold larger absorption capability of canopies as compared to the absorption of Chl in vitro, where the absorption coefficient in the green and red-edge spectral regions does not exceed 1–1.5% of the amplitude of the red absorption maximum (Lichtenthaler, 1983). Another feature of canopy $(\rho_\lambda)^{-1}$ spectra is represented by positive values in the near infrared (NIR) region, beyond 760 nm, where Chl *a* and *b* do not absorb light. The absorption of healthy leaves in the NIR region is negligible, while that of canopies is sizeable due to either apparent absorption (i.e., fraction of light transmitted through the canopy) and/or due to the presence of other absorbers such as 'brown' pigments produced upon the oxidation of polyphenols during leaf damage or senescence (Merzlyak et al., 2002; Merzlyak et al., 2004).

The $(\rho_\lambda)^{-1}$ spectra show that the canopy absorption coefficient $\alpha_{pigm}$ estimated via $(\rho_\lambda)^{-1}$ (Eq. (3)) may be biased especially (i) in spectral regions of small pigment absorption where $\alpha_{pigm}$ is comparable to $\alpha_0$, specifically in the green and red edge where it may exceed 10–15% of $\alpha_{pigm}$, and (ii) at the beginning and at the end of the growing season when total absorption is small-to-moderate. Subtraction of reciprocal reflectance in the NIR, $\rho_{NIR}^{-1}$, eliminates or at least significantly decreases $a_0$ in the numerator of Eq. (3):

$$(\rho_\lambda^{-1} - \rho_{NIR}^{-1}) \propto \tilde{\alpha}_{pigm}(\lambda)/\beta \quad (4)$$

The absorption coefficient, $\alpha_{pigm}$, retrieved from Eq. (4), for canopies having the same pigment content but different densities (e.g., LAI, biomass) may be biased due to different values of the scattering coefficient, $\beta$, in the denominator of Eq. (4). This effect may be quite significant. For example, a crop in the vegetative stage may have the same canopy pigment content as another crop in the reproductive stage; both will differ with regards to their LAI values and foliar pigment content (i.e., higher foliar pigment content and smaller LAI in vegetative stage and vice versa in reproductive stage). As a result, for the same

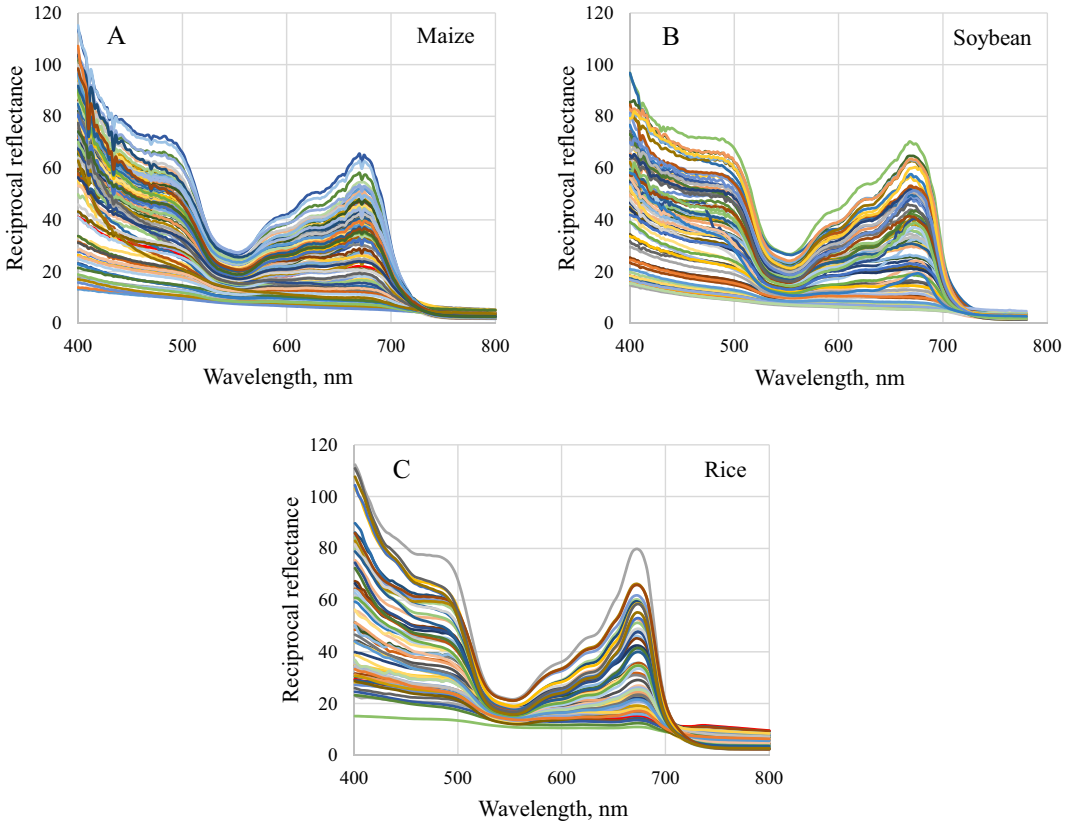


**Fig. 2.** Reciprocal reflectance spectra of (A) maize, (B) soybean and (C) rice canopies.

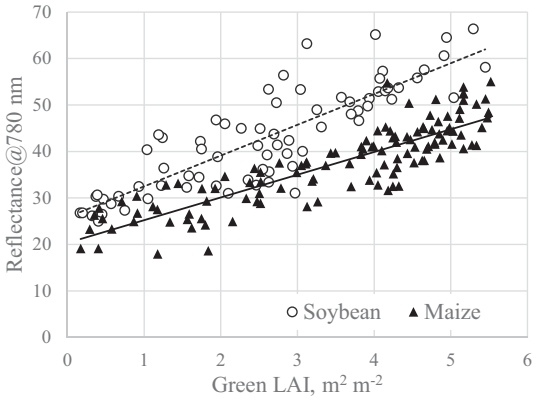


**Fig. 3.** Relationships between NIR reflectance at 780 nm and green leaf area index in maize and soybean canopies.

canopy pigment content, in accord with Eq. (4), the retrieved $\alpha_{pigm}$ would be larger in the vegetative stage (due to smaller LAI and thus canopy scattering coefficient β) than in the reproductive stage. This effect may be reduced, if not eliminated, using reflectance that roughly represents canopy scattering coefficient but is not affected by pigment absorption. Reflectance in the NIR region, where chlorophylls do not absorb, is closely related with canopy structural properties (e.g., LAI - Fig. 3). The higher NIR reflectance in soybean than in maize is mainly due to differences in canopy architecture, including leaf angle distribution (i.e., planophile vs. spherical leaf angle distributions) and leaf structure. Thus, canopy density is not the only factor defining NIR reflectance. It is also affected by the leaf angle distribution and leaf structure (as shown in Fig. 3) as well as soil background. To decrease the effect of differential scattering in canopies with the same [Chl] and isolate $\alpha_{pigm}$, $\rho_{NIR}$ is introduced in Eq. (4):

$$\tilde{a}_{pigm}(\lambda) \propto [(\rho_\lambda)^{-1}-(\rho_{NIR})^{-1}) \times \rho_{NIR} = (\rho_{NIR}/\rho_\lambda - 1) \quad (5)$$

This model (Eq. (5)) describes the total canopy absorption coefficient. Below we evaluate the ability of this model to retrieve the canopy-level absorption coefficient of Chl in three crops (maize, soybean and rice) with different structural, biochemical, and functional traits.

## 3. Materials and methods

### 3.1. Study areas

Maize and soybeans were studied between 2001 and 2008 in research fields (AmeriFlux sites US-Ne1, US-Ne1, and US-Ne3) owned and operated by the University of Nebraska-Lincoln's Eastern Nebraska Research and Extension Center located near Mead, Nebraska, U.S.A. Rice was studied during 2009 in experimental fields owned and operated by the National Institute for Agro-Environmental Studies (NIAES) and located in Tsukuba, Japan. Details of these different research fields (including crop cultural practices) are given in Viña et al. (2011) and Inoue et al. (2016).

### 3.2. Canopy reflectance

Canopy reflectance spectra of maize, soybeans and rice were obtained close to solar noon (between 10:00 and 13:00 local time), when changes in solar zenith angle were minimal. Measurements in the first two crops were performed using two Ocean Optics USB2000 spectroradiometers mounted on an all-terrain platform. Details of the procedures used are given in Rundquist et al. (2014), Rundquist et al. (2004), and Viña et al. (2011). Measurements in rice were performed using a FieldSpec-Pro ASD spectroradiomenter. Details of the procedures employed are given in Inoue et al. (2016).

### 3.3. Green leaf area index

Destructive estimations of green leaf area per plant were obtained in the lab from samples collected in maize, soybeans and rice fields using an area meter (LI-3100, Li-Cor, Inc., Lincoln, Nebraska). To obtain a per-field green LAI, these measurements were multiplied by plant populations obtained in the fields. Details of these procedures are given in Law et al. (2008), Viña et al. (2011), and Inoue et al. (2016).

### 3.4. Chlorophyll content

Spectral reflectance measurements of the ear leaf in maize and the most recently fully expanded leaf in soybean were obtained every two weeks in the maize and soybean sites using an Ocean Optics USB2000 radiometer. The leaves were collected from the same plants in which canopy reflectance was measured. These leaves were then transported to a lab where leaf Chl content ($[Chl]_{leaf}$) was determined analytically as detailed in Gitelson et al. (2006a). A linear model was obtained relating $[Chl]_{leaf}$ with the Red Edge Chlorophyll Index ($CI_{red\ edge}$) ($R^2 = 0.95$):

$$[Chl]_{leaf}\ (mg\ m^{-2}) = 37.904 + 1353.7 \times CI_{red\ edge} \quad (6)$$

where $CI_{red\ edge} = (\rho_{NIR}/\rho_{red\ edge}) - 1$, $\rho_{NIR}$ is reflectance in the near infrared spectral region (between 770 nm and 800 nm), and $\rho_{red\ edge}$ is reflectance in the red-edge spectral region (between 720 nm and 730 nm). This model was validated for maize and soybean leaves and was shown to be non-species-specific with a root mean squared error (RMSE) lower than 61 mg $m^{-2}$ (see Ciganda et al., 2009). Using this model, $Chl_{leaf}$ was calculated for all maize and soybean leaves sampled. Canopy [Chl] for each field was then calculated as the product of $Chl_{leaf}$ and per-field green LAI (Ciganda et al., 2009; Gitelson et al., 2005). In rice, leaves for Chl measurements were collected from the same plants in which canopy reflectance was measured. $[Chl]_{leaf}$ was extracted with 90% acetone, and determined through absorption spectroscopy (using a Shimadzu UV-1600 GLP spectrophotometer) and coefficients published in Lichtenthaler (1987). Canopy [Chl] was then obtained as the product of $[Chl]_{leaf}$ and the biomass of green leaves per $m^2$ in the canopy (Morita, 1978). Statistics of canopy chlorophyll content in the crops studied are given in Table 1.

### 3.5. Assessing uncertainties of absorption coefficient retrieval

To assess the accuracy of Chl absorption coefficient retrieval from reflectance spectra, the noise equivalent of $\alpha_{chl}$ ($NE\alpha_{chl}$) was calculated as (Viña and Gitelson, 2005):

$$NE\alpha_{chl} = NRMSE\{\alpha_{chl}\ vs.\ canopy\ [Chl]\}/[d(\alpha_{chl})/d(canopy\ [Chl])] \quad (7)$$

where $d(\alpha_{chl})/d(canopy\ [Chl])$ is the first derivative of the linear relationship between $\alpha_{chl}$ and canopy [Chl], and $NRMSE\{\alpha_{chl}$ vs. canopy [Chl]$\}$ is the normalized root mean squared error of this relationship. Calculated in percent, $NE\alpha_{chl}$ was used to evaluate the accuracy of $\tilde{a}_{chl}(\lambda)$ estimation in vegetation with different canopy [Chl].

## 4. Results and discussion

The pivotal question we needed to answer was whether it is possible to isolate the absorption coefficient of pigment α (i.e., $\alpha_{chl}$) from the scattering coefficient β in media where both factors affect reflectance. To answer this question, we used the total canopy [Chl] (i.e., the product of leaf [Chl] and green LAI) of three crops, measured in situ. We quantified the effect of canopy [Chl] on three functions of reflectance, $f_i(\rho)$: reciprocal reflectance ($\rho_\lambda{}^{-1}$) – Eq. (3), the difference ($\rho_\lambda{}^{-1} - \rho_{NIR}{}^{-1}$) – Eq. (4). and apparent Chl absorption coefficient $\tilde{a}_{chl}(\lambda) = (\rho_{NIR}/\rho_\lambda - 1)$ – Eq. (5). Relationships between [Chl] and these three functions of reflectance were established at each wavelength (λ) and for each crop. The effect of canopy [Chl] on $f_i(\rho)$, termed *response function* (Gitelson and Solovchenko, 2017), was calculated as the ratio of the first derivative to the root mean squared error (RMSE) of the $f_i(\rho)$ vs. [Chl] relationship (Viña and Gitelson, 2005):

$$Rf(\rho),\ m^2\ g^{-1} = (df_i(\rho)/d[Chl])/RMSE \quad (8)$$

where the numerator represents sensitivity of $f_i(\rho)$ to [Chl] in g $m^{-2}$ and the denominator is a measure of noise. Thus, the $Rf_i(\rho)$ represents a quantitative measure of the $f_i(\rho)$ response to [Chl] that combines the sensitivity of the function to [Chl] and the accuracy of the [Chl] assessment. The response $Rf_i(\rho)$ to [Chl] in three disparate crops evaluates how close to linear the $f_i(\rho)$ vs. [Chl] relationship is, how sensitive $f_i(\rho)$ is to [Chl] and, therefore, if $f_i(\rho_{NIR}/\rho_\lambda - 1)$ indeed represents the canopy Chl absorption coefficient, $\alpha_{chl}$ (Fig. 4).

$R\rho_\lambda{}^{-1}$ in the three studied crops have several common spectral features: a peak in the green edge region of the visible portion of the electromagnetic spectrum (ca. 520 nm), a minimum in the green region (around 560 nm), maximal values around 690–700 nm and a sharp drop toward longer wavelengths in the red edge region. There was no response of $R\rho_\lambda{}^{-1}$ to [Chl] when scattering by the canopy offset the Chl absorption. This happens in maize and soybean at around 730 nm while in rice, having lower [Chl], this occurs at a shorter wavelength (ca. 700 nm). Toward longer wavelengths (i.e., in the red edge and NIR spectral regions), scattering by the canopy constitutes the main factor governing reflectance, thus the responses become negative (not shown in Fig. 4). Importantly, while the in vivo Chl absorption coefficient in the green range is about 1–2% of that in the blue and the red regions (Lichtenthaler, 1987), $R\rho_\lambda{}^{-1}$ in the green range is comparable to the responses in the blue and red for maize and soybean. The lower rice canopy [Chl] caused a pronounced minimum of $R\rho_\lambda{}^{-1}$ in the green range.

Subtraction of reciprocal reflectance in the NIR (beyond 760 nm) allows eliminating $\alpha_0$ from the numerator of Eq. (3) and better isolating the absorption coefficient (Eq. (4)). The spectral response of $R(\rho_\lambda{}^{-1} - \rho_{NIR}{}^{-1})$ to [Chl] was higher than that of $R\rho_\lambda{}^{-1}$ in the green, particularly in rice, due to lower canopy [Chl] than in other crops (Table 1); $\rho_\lambda{}^{-1}$ in the green spectral region being small and greatly affected by the variability of $\rho_{NIR}{}^{-1}$ (Fig. 4). In all crops, the response $R(\rho_\lambda{}^{-1} - \rho_{NIR}{}^{-1})$ was further enhanced beyond the PAR region at wavelengths 50–70 nm away from the main in situ red Chl absorption band centered around 680 nm. This means that at the canopy scale, the absorption peak of Chl is quite wide, producing high absorption in the red-edge region at 730–740 nm.

The next step for isolating the absorption coefficient was to remove the effect of canopy backscattering. This was achieved by multiplying $(\rho_\lambda^{-1} - \rho_{NIR}{}^{-1})$ by $\rho_{NIR}$, which compensates for the overestimation of $\alpha_{chl}$ due to smaller LAI and for the underestimation of $\alpha_{chl}$ due to larger LAI (Eq. (5)). This brought about an increase in $R\tilde{a}_{chl}(\lambda)$ to [Chl] in all three crops (Fig. 4). The highest effect of scattering variability in canopies with the same [Chl] took place in the green and the red edge due to smaller foliar Chl absorption coefficients in these spectral regions. Thus, decreasing (if not eliminating) the backscattering effect resulted in a significant increase in the response of $\tilde{a}_{chl}(\lambda)$ to [Chl] in these spectral ranges. Notably, $R\tilde{a}_{chl}(\lambda)$ peaked in the green and the red edge regions and were minimal in the main absorption bands of Chl, the blue and red regions.

The apparent absorption coefficient in the blue, green, red, and red

**Table 1**
Minimal, maximal, average and median canopy chlorophyll contents (in g $m^{-2}$) in crops studied.

| | Min | Max | Average | Median |
|---|---|---|---|---|
| Maize | 0.07 | 3.61 | 2.04 | 2.13 |
| Soybean | 0.03 | 2.79 | 1.00 | 0.86 |
| Rice | 0.01 | 2.13 | 0.63 | 0.53 |

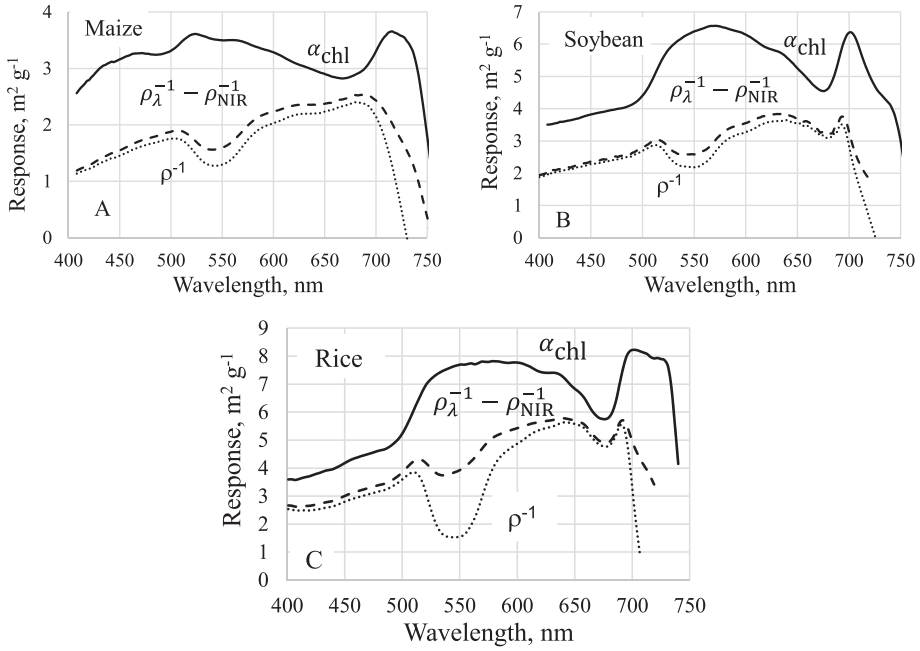


**Fig. 4.** Spectral response of three functions of reflectance, $(\rho_\lambda{}^{-1})$, $(\rho_\lambda{}^{-1}-\rho_{NIR}{}^{-1})$, and $\tilde{a}_{chl}(\lambda) = (\rho_{NIR}/\rho_\lambda - 1)$, to canopy [Chl] in (A) maize, (B) soybean, and (C) rice.

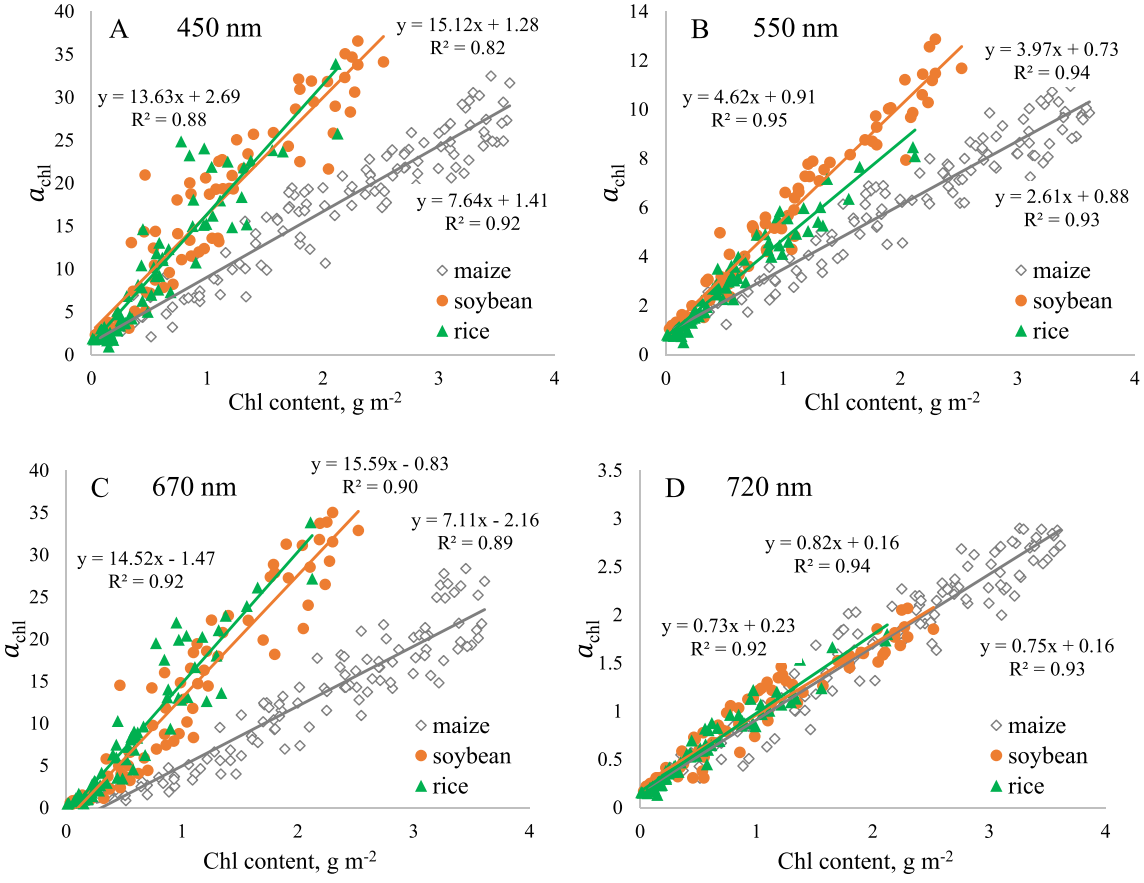


**Fig. 5.** Relationships between retrieved apparent absorption coefficient of canopy chlorophyll $\tilde{a}_{chl}(\lambda)$ and measured canopy chlorophyll content. Data were taken at three irrigated and rainfed maize and soybean sites in 2001–2008 and at a rice site in 2009. (For interpretation of the references to colour in this figure legend, the reader is referred to the web version of this article.)

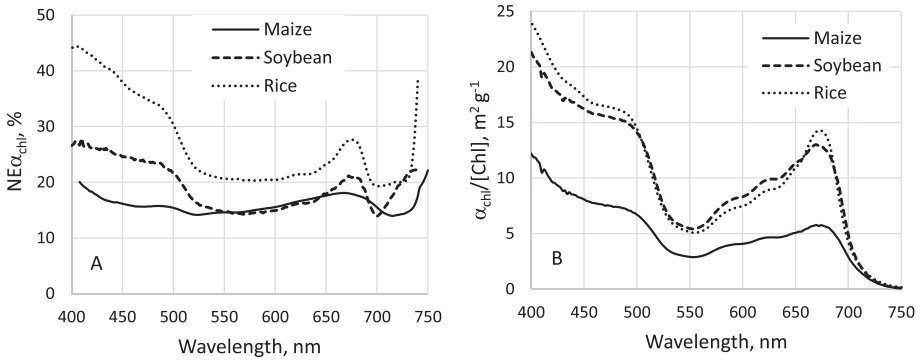


**Fig. 6.** (A) Noise equivalent of absorption coefficient $\tilde{a}_{chl}(\lambda)$ estimation by the model $(\rho_{nir}/\rho_{\lambda}) - 1$, (Eq. (5)), and (B) absorption coefficient spectra of chlorophyll, $\tilde{a}_{chl}(\lambda)$/[Chl], in three crops - maize, soybean, and rice.

edge spectral regions related closely to canopy [Chl] (Fig. 5). The determination coefficient, $R^2$, of $\tilde{a}_{chl}(\lambda)$ vs. [Chl] relationships constitutes a quantitative measure of how well $\tilde{a}_{chl}(\lambda)$ performs as a predictor of [Chl] and how much of $\tilde{a}_{chl}(\lambda)$ variability can be explained by [Chl] variation. The slopes of these relationships (Fig. 5) represent the sensitivity of $\tilde{a}_{chl}(\lambda)$ to [Chl]. The relationships were very close to linearity along the entire PAR and red edge regions in all crops, with high $R^2$, while the slopes of the relationships varied: highest was for rice and lowest for maize. Nevertheless, none of these characteristics, $R^2$ or d $(\tilde{a}_{chl}(\lambda)/d[Chl]$, constitutes an accurate quantitative measure of $\tilde{a}_{chl}(\lambda)$ retrieval accuracy by Eq. (5). This is because the slopes per se do not imply the strength of the corresponding relationships and the $R^2$ bears no information about the sensitivity of $\tilde{a}_{chl}(\lambda)$ to [Chl]. Thus, we used the noise equivalent (Eq. (7)) as a measure of the accuracy of the retrieval of the apparent absorption coefficient, $\tilde{a}_{chl}(\lambda)$, from reflectance spectra (Fig. 6A).

The noise equivalent of the $\tilde{a}_{chl}(\lambda)$ estimation for the crops studied had minimal values in the green and red edge spectral regions, varying between 20% (rice) and below 15% (maize and soybean) - Fig. 6A. NE$\tilde{a}_{chl}(\lambda)$ was higher in the blue region where chlorophylls, carotenoids, and flavonoids absorb and total pigment absorption is maximal (Fig. 6B). Across the entire PAR and red edge regions, the NE$\tilde{a}_{chl}(\lambda)$ was below 20% in maize and below 30% in soybean, while it was larger in rice, especially in the blue region where it exceeded 40%. The background reflectance of the rice canopy is lower than in other crops due mainly to the presence of a layer of shallow water on the soil background (Kimura et al., 2004; Shibayama and Akiyama, 1989). In the blue region, the soil/water background reflectance was below 5%, which is at least two times smaller than in both maize and soybean (Fig. 1S). At early stages of rice development, water strongly contributed to the background reflectance. An indication of this is the pronounced peak around 700 nm (Fig. 2S) - the product of decreasing absorption by Chl and increasing water absorption in this spectral region (Gitelson, 1992). Thus, discrepancies between $\tilde{a}_{chl}(\lambda)$ and [Chl] in the blue spectral region between rice and maize/soybean are due to the absorption exerted by open water in the soil background; so in the entire dynamic range of [Chl], the blue reflectance change was very small (below 3%). Despite this, in the range 530–740 nm the NE$\tilde{a}_{chl}$ vs. $\lambda$ relationship exhibited a small variability, which allows for the estimation of $\tilde{a}_{chl}$ in maize and soybean with a NE$\tilde{a}_{chl}$ below 20% and below 30% in rice.

The shapes of the apparent specific Chl absorption coefficient spectra, $\tilde{a}_{chl}(\lambda)$/[Chl], were quite close for the crops studied, however, the magnitudes were significantly different for C3 and C4 crops (Fig. 6B). $\tilde{a}_{chl}(\lambda)$/[Chl] was higher in soybean and rice (C3 crops) than in maize (C4 crop), indicating that soybean and rice canopies with the same [Chl] absorb more radiation than maize canopies. For the same dataset as the one used in this paper, it was shown that: (i) for the same canopy [Chl] gross primary production (GPP) in maize and soybean were almost equal (Gitelson et al., 2016; Gitelson et al., 2006b); and (ii) the light use efficiency (LUE) of photosynthetically active components of the maize canopy was significantly higher than that of soybean: $LUE_{maize}/LUE_{soybean} = 1.61$ (Gitelson et al., 2018; Gitelson et al., 2016). The LUE of the photosynthetically active fraction of vegetation was defined as $LUE_{green} = GPP/APAR_{green}$, where $APAR_{green}$ is radiation absorbed by the photosynthetically active vegetation (Gitelson et al., 2018; Gitelson and Gamon, 2015). These results imply that for the C3 plant to have a GPP equal to that of the C4 plant, it has to absorb more light; conversely, for a given amount of light absorbed, the C3 plant canopy has a lower net $CO_2$ assimilation rate (and, hence, GPP) than a C4 plant canopy. This is largely due to photorespiration (loss of $CO_2$) in C3 plants caused by the oxygenase reaction of Rubisco. C4 plants avoid appreciable photorespiration by concentrating $CO_2$ at the Rubisco active site. In the calculation of GPP, regular respiration adds to the total GPP (GPP = net $CO_2$ assimilation + respiration) but photorespiration does not (since it is already included in the 'net $CO_2$ assimilation' term). Thus, for the same radiation absorbed by photosynthetically active vegetation (i.e., for the same [Chl]), GPP would be higher in C4 plant canopies.

The model proposed here allowed us to pinpoint the above mentioned differences in light capture between C3 and C4 plants making it possible to test the accuracy of $\tilde{a}_{chl}(\lambda)$/[Chl] retrieval for maize and soybean from reflectance spectra along the entire PAR region. The ultimate confirmation of this would be the ability to accurately predict the differences in LUE related to different photosynthetic mechanisms in maize and soybean. This can be done via the total canopy absorption $APAR_{green}$ of these crops calculated using the developed model. To this effect, we compared the integral of $\tilde{a}_{chl}(\lambda)$/[Chl] of maize and soybean across the PAR region (400–700 nm) and found the ratio $APAR_{soybean}/APAR_{maize} = 1.64$. The ratios $APAR_{soybean}/APAR_{maize}$ and $LUE_{maize}/LUE_{soybean}$ were almost equal (their difference was smaller than the estimation errors of $LUE_{green}$ and $APAR_{green}$). Thus, deriving an absorption coefficient from reflectance spectra in crop canopies allows quantification of a fundamental difference in the light energy utilization mechanisms of C3 and C4 plant canopies. This approach demonstrates the possibility of using the retrieved $\tilde{a}_{chl}(\lambda)$ to accurately quantify canopy absorption as well as other vegetation traits across the entire PAR region. This may be considered as an additional confirmation of the accuracy of apparent absorption coefficient isolation by the model described in Eq. (5).

The spectra of NE$\tilde{a}_{chl}(\lambda)$ (Fig. 6A) indicate the spectral regions with minimal uncertainties of $\tilde{a}_{chl}(\lambda)$ estimation in each crop: a wide green region (520–620 nm) and a red edge region (710–740 nm). Importantly, these spectra also indicated that for all data (maize, soybean and rice) taken together, $\tilde{a}_{chl}(\lambda)$ in the green range did not match [Chl], thus, this range is not suitable for generic [Chl] estimation in the three crops. The only spectral range that could be used for a generic estimation of [Chl] is the red edge region where $\tilde{a}_{chl}(\lambda)$ in all three crops converged

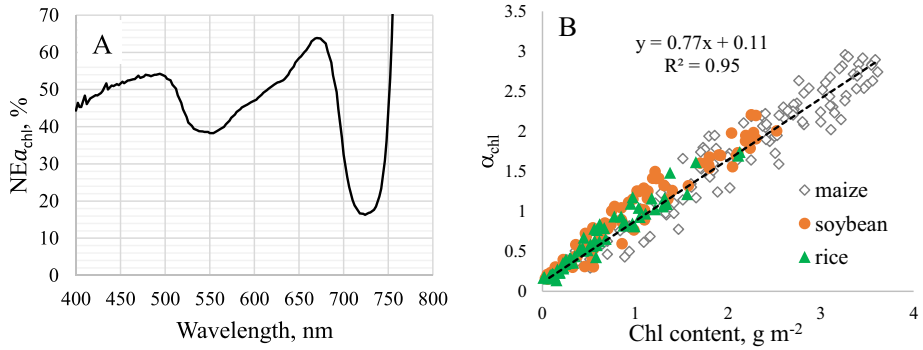


**Fig. 7.** (A) Noise equivalent of the absorption coefficient $\tilde{a}_{chl}(\lambda)$ estimation by the model Eq. (5), retrieved from in situ reflectance spectra plotted versus wavelength for three crops taken together. (B) Absorption coefficient of Chl in the range 710–740 nm plotted vs. Chl content in maize, soybean and rice.

**Table 2**
Algorithms and normalized root mean squared errors of [Chl] estimation by the absorption coefficient of Chl, $\tilde{a}_{chl}(\Delta\lambda)$, retrieved from in situ reflectance spectra in the spectral range $\Delta\lambda$, and by the MERIS terrestrial chlorophyll index (MTCI).

| $\Delta\lambda$ | Algorithm | NRMSE, % |
|---|---|---|
| $\tilde{a}_{chl}$(710–740) | [Chl] = 1.94 $\tilde{a}_{chl}$ – 0.25 | 19.01 |
| $\tilde{a}_{chl}$(732–748) MSI | [Chl] = 7.03 $\tilde{a}_{chl}$ – 0.47 | 16.46 |
| MTCI(704–714) MSI | [Chl] = 0.28 MTCI – 0.28 | 21.12 |

(Fig. 6B). We calculated a NE$\tilde{a}_{chl}(\lambda)$ spectrum for the three crops considered together (Fig. 7A) showing a pronounced minimum of NE$\tilde{a}_{chl}(\lambda)$ in the spectral range 710–740 nm. This indicates that $\tilde{a}_{chl}(\lambda)$ (Eq. (5)) in this region allows for the estimation of [Chl] in all three crops with a single parameterization. Fig. 7B shows that in the range 710–740 nm $\tilde{a}_{chl}$ explains 95% of [Chl] variation. As seen in Table 2, $\tilde{a}_{chl}(\lambda)$ retrieved from reflectance spectra was suitable for estimating [Chl] in the three crops with NRMSE below 20%. It is also notable that $\tilde{a}_{chl}$ calculated in the simulated spectral band 732–748 nm of the Multispectral Instrument (MSI) onboard Sentinel 2 brought an accurate estimation of [Chl] in the three crops evaluated (NRMSE < 17%), over performing the MERIS terrestrial chlorophyll index (MTCI) (Dash and Curran, 2007,Dash and Curran, 2004) calculated using the spectral bands of the MSI.

## 5. Conclusion

The spectra of canopy Chl absorption coefficients in the PAR and red edge regions derived from canopy reflectance spectra bring important information about the canopy-level physiological and phenological status of plants as well as about their photosynthetic capacity. The two important outputs of this work are (i) a generic model for the retrieval of the chlorophyll absorption coefficient in canopies with disparate structural properties (LAI and leaf angle distribution), biochemistries (pigment content and composition) and photosynthetic pathways (C3 vs. C4), and (ii) the method of quantification of the canopy [Chl] without the need of re-parameterization for each canopy type. While the model was designed to retrieve the total absorption coefficient of pigments, in this study it was used to evaluate the absorption coefficient of canopy Chl. In the crops studied the foliar [Chl] was closely related to the carotenoid content (Gitelson and Solovchenko, 2017), while the plants studied were anthocyanin-free, thus the total canopy absorption coefficient in our case indeed represented the Chl absorption coefficient.

## Acknowledgements

Funding by the Russian Foundation for Basic Research (AS) is gratefully acknowledged (project 19-016-00016). This publication was prepared with the support of the «RUDN University Program 5-100». The work was also supported, in part, by the USDA National Institute of Food and Agriculture Hatch project No. 1002649.

## Appendix A. Supplementary data

Supplementary data to this article can be found online at https://doi.org/10.1016/j.rse.2019.111276.

## References

Asner, G.P., Martin, R.E., Anderson, C.B., Knapp, D.E., 2015. Quantifying forest canopy traits: imaging spectroscopy versus field survey. Remote Sens. Environ. 158, 15–27.
Blackburn, G.A., 2006. Hyperspectral remote sensing of plant pigments. J. Exp. Bot. 58, 855–867.
Burke, M., Lobell, D.B., 2017. Satellite-based assessment of yield variation and its determinants in smallholder African systems. Proc. Natl. Acad. Sci. 114, 2189–2194.
Chen, M., 2014. Chlorophyll modifications and their spectral extension in oxygenic photosynthesis. Annu. Rev. Biochem. 83, 317–340.
Ciganda, V., Gitelson, A., Schepers, J., 2009. Non-destructive determination of maize leaf and canopy chlorophyll content. J. Plant Physiol. 166, 157–167.
Croce, R., Van Amerongen, H., 2014. Natural strategies for photosynthetic light harvesting. Nat. Chem. Biol. 10, 492.
Dash, J., Curran, P.J., 2004. The MERIS terrestrial chlorophyll index. Int. J. Remote Sens. 25, 5403–5413.
Dash, J., Curran, P., 2007. Evaluation of the MERIS terrestrial chlorophyll index (MTCI). Adv. Space Res. 39, 100–104.
Deines, J.M., Kendall, A.D., Hyndman, D.W., 2017. Annual irrigation dynamics in the US northern high plains derived from Landsat satellite data. Geophys. Res. Lett. 44, 9350–9360.
Drusch, M., Del Bello, U., Carlier, S., Colin, O., Fernandez, V., Gascon, F., Hoersch, B., Isola, C., Laberinti, P., Martimort, P., 2012. Sentinel-2: ESA's optical high-resolution mission for GMES operational services. Remote Sens. Environ. 120, 25–36.
Fahey, D.W., Doherty, S., Hibbard, K.A., Romanou, A., Taylor, P., 2017. Physical drivers of climate change. In: Wuebbles, D.J., Fahey, D.W., Hibbard, K.A., Dokken, D.J., Stewart, B.C., Maycock, T.K. (Eds.), Climate Science Special Report: A Sustained Assessment Activity of the U.S. Global Change Research Program. U.S. Global Change Research Program, Washington DC, USA, pp. 98–159.
Frankenberg, C., O'Dell, C., Berry, J., Guanter, L., Joiner, J., Köhler, P., Pollock, R., Taylor, T.E., 2014. Prospects for chlorophyll fluorescence remote sensing from the Orbiting Carbon Observatory-2. Remote Sens. Environ. 147, 1–12.
Friend, A.D., 2010. Terrestrial plant production and climate change. J. Exp. Bot. 61, 1293–1309.
Gamon, J.A., Field, C.B., Goulden, M.L., Griffin, K.L., Hartley, A.E., Joel, G., Penuelas, J., Valentini, R., 1995. Relationships between NDVI, canopy structure, and photosynthesis in three Californian vegetation types. Ecol. Appl. 5, 28–41.
Gholizadeh, H., Robeson, S.M., Rahman, A.F., 2015. Comparing the performance of multispectral vegetation indices and machine-learning algorithms for remote estimation of chlorophyll content: a case study in the Sundarbans mangrove forest. Int. J. Remote Sens. 36, 3114–3133.
Gitelson, A., 1992. The peak near 700 nm on radiance spectra of algae and water: relationships of its magnitude and position with chlorophyll concentration. Int. J. Remote Sens. 13, 3367–3373.
Gitelson, A.A., Gamon, J.A., 2015. The need for a common basis for defining light-use efficiency: implications for productivity estimation. Remote Sens. Environ. 156, 196–201.
Gitelson, A., Solovchenko, A., 2017. Generic algorithms for estimating foliar pigment content. Geophys. Res. Lett. 44, 9293–9298.
Gitelson, A.A., Viña, A., Ciganda, V., Rundquist, D.C., Arkebauer, T.J., 2005. Remote estimation of canopy chlorophyll content in crops. Geophys. Res. Lett. 32.
Gitelson, A.A., Keydan, G.P., Merzlyak, M.N., 2006a. Three-band model for noninvasive

estimation of chlorophyll, carotenoids, and anthocyanin contents in higher plant leaves. Geophys. Res. Lett. 33.
Gitelson, A.A., Viña, A., Verma, S.B., Rundquist, D.C., Arkebauer, T.J., Keydan, G., Leavitt, B., Ciganda, V., Burba, G.G., Suyker, A.E., 2006b. Relationship between gross primary production and chlorophyll content in crops: implications for the synoptic monitoring of vegetation productivity. J. Geophys. Res. Atmos. 111.
Gitelson, A.A., Viña, A., Masek, J.G., Verma, S.B., Suyker, A.E., 2008. Synoptic monitoring of gross primary productivity of maize using Landsat data. IEEE Geosci. Remote Sens. Lett. 5, 133–137.
Gitelson, A.A., Peng, Y., Viña, A., Arkebauer, T., Schepers, J.S., 2016. Efficiency of chlorophyll in gross primary productivity: a proof of concept and application in crops. J. Plant Physiol. 201, 101–110.
Gitelson, A.A., Arkebauer, T.J., Suyker, A.E., 2018. Convergence of daily light use efficiency in irrigated and rainfed C3 and C4 crops. Remote Sens. Environ. 217, 30–37.
Guanter, L., Frankenberg, C., Dudhia, A., Lewis, P.E., Gómez-Dans, J., Kuze, A., Suto, H., Grainger, R.G., 2012. Retrieval and global assessment of terrestrial chlorophyll fluorescence from GOSAT space measurements. Remote Sens. Environ. 121, 236–251.
Hanan, N.P., Burba, G., Verma, S.B., Berry, J.A., Suyker, A., Walter-Shea, E.A., 2002. Inversion of net ecosystem CO2 flux measurements for estimation of canopy PAR absorption. Glob. Chang. Biol. 8, 563–574.
Houborg, R., McCabe, M., Cescatti, A., Gao, F., Schull, M., Gitelson, A., 2015. Joint leaf chlorophyll content and leaf area index retrieval from Landsat data using a regularized model inversion system (REGFLEC). Remote Sens. Environ. 159, 203–221.
Inoue, Y., Guérif, M., Baret, F., Skidmore, A., Gitelson, A., Schlerf, M., Darvishzadeh, R., Olioso, A., 2016. Simple and robust methods for remote sensing of canopy chlorophyll content: a comparative analysis of hyperspectral data for different types of vegetation. Plant Cell Environ. 39, 2609–2623.
Joiner, J., Yoshida, Y., Vasilkov, A., Schaefer, K., Jung, M., Guanter, L., Zhang, Y., Garrity, S., Middleton, E., Huemmrich, K., 2014. The seasonal cycle of satellite chlorophyll fluorescence observations and its relationship to vegetation phenology and ecosystem atmosphere carbon exchange. Remote Sens. Environ. 152, 375–391.
Kimura, R., Okada, S., Miura, H., Kamichika, M., 2004. Relationships among the leaf area index, moisture availability, and spectral reflectance in an upland rice field. Agric. Water Manag. 69, 83–100.
Kortum, G., 1969. Reflectance Spectroscopy. Principles, Methods, Applications. Springler-Verlag Inc., New York, NY.
Kubelka, P., Munk, F., 1931. Ein Beitrag Zur Optik Der Farbanstriche. Z. Tech. Phys. 12, 593–601.
Law, B.E., Arkebauer, T., Campbell, J.L., Chen, J., Sun, O., Schwartz, M., van Ingen, C. & Verma S. (2008). Terrestrial Carbon Observations: Protocols for Vegetation Sampling and Data Submission. Global Terrestrial Observing System, FAO, Rome, Report 55, 87.
Li, Y., Liu, C., Zhang, J., Yang, H., Xu, L., Wang, Q., Sack, L., Wu, X., Hou, J., He, N., 2018. Variation in leaf chlorophyll concentration from tropical to cold-temperate forests: association with gross primary productivity. Ecol. Indic. 85, 383–389.
Lichtenthaler, H., 1983. Differences in chlorophyll levels, fluorescence and photosynthetic activity of leaves from high-light and low-light seedlings. In: Metzner, H. (Ed.), Photosynthesis and Plant Productivity: Joint Meeting of OECD and Studienzentrum Weikersheim, Ettlingen Castle (Germany), October 11–14, 1981. Wissenschaftliche Verlagsgesellschaft, Stuttgart.
Lichtenthaler, H.K., 1987. Chlorophylls and Carotenoids: Pigments of Photosynthetic Biomembranes. *Methods in* Enzymology. Elsevier, pp. 350–382.
Luo, X., Croft, H., Chen, J.M., Bartlett, P., Staebler, R., Froelich, N., 2018. Incorporating leaf chlorophyll content into a two-leaf terrestrial biosphere model for estimating carbon and water fluxes at a forest site. Agric. For. Meteorol. 248, 156–168.
Merzlyak, M.N., Chivkunova, O.B., Melø, T., Naqvi, K.R., 2002. Does a leaf absorb radiation in the near infrared (780–900 nm) region? A new approach to quantifying optical reflection, absorption and transmission of leaves. Photosynth. Res. 72, 263–270.
Merzlyak, M.N., Melø, T., Naqvi, K.R., 2004. Estimation of leaf transmittance in the near infrared region through reflectance measurements. J. Photochem. Photobiol. B Biol. 74, 145–150.
Morita, K., 1978. A physiological study on the dynamic status of leaf nitrogen in rice plants. Bull Hokuriku Natl Agric Exp Stn 21, 1–61.
Peng, Y., Gitelson, A.A., Keydan, G., Rundquist, D.C., Moses, W., 2011. Remote estimation of gross primary production in maize and support for a new paradigm based on total crop chlorophyll content. Remote Sens. Environ. 115, 978–989.
Peng, Y., Nguy-Robertson, A., Arkebauer, T., Gitelson, A.A., 2017. Assessment of canopy chlorophyll content retrieval in maize and soybean: implications of hysteresis on the development of generic algorithms. Remote Sens. 9, 226.
Piao, S., Fang, J., Zhou, L., Zhu, B., Tan, K., Tao, S., 2005. Changes in vegetation net primary productivity from 1982 to 1999 in China. Glob. Biogeochem. Cycles 19.
Richardson, A.D., Duigan, S.P., Berlyn, G.P., 2002. An evaluation of noninvasive methods to estimate foliar chlorophyll content. New Phytol. 153, 185–194.
Rundquist, D., Perk, R., Leavitt, B., Keydan, G., Gitelson, A., 2004. Collecting spectral data over cropland vegetation using machine-positioning versus hand-positioning of the sensor. Comput. Electron. Agric. 43, 173–178.
Rundquist, D., Gitelson, A., Leavitt, B., Zygielbaum, A., Perk, R., Keydan, G., 2014. Elements of an integrated phenotyping system for monitoring crop status at canopy level. Agronomy 4, 108–123.
Shibayama, M., Akiyama, T., 1989. Seasonal visible, near-infrared and mid-infrared spectra of rice canopies in relation to LAI and above-ground dry phytomass. Remote Sens. Environ. 27, 119–127.
Sippel, S., Reichstein, M., Ma, X., Mahecha, M.D., Lange, H., Flach, M., Frank, D., 2018. Drought, heat, and the carbon cycle: a review. Current Climate Change Reports 1–21.
Sun, J., Shi, S., Yang, J., Chen, B., Gong, W., Du, L., Mao, F., Song, S., 2018. Estimating leaf chlorophyll status using hyperspectral lidar measurements by PROSPECT model inversion. Remote Sens. Environ. 212, 1–7.
Ustin, S.L., Gamon, J.A., 2010. Remote sensing of plant functional types. New Phytol. 186, 795–816.
Viña, A., 2004. Remote Estimation of Leaf Area Index and Biomass in Corn and Soybean. PhD Dissertation. University of Nebraska-Lincoln.
Viña, A., Gitelson, A.A., 2005. New developments in the remote estimation of the fraction of absorbed photosynthetically active radiation in crops. Geophys. Res. Lett. 32.
Viña, A., Gitelson, A.A., Nguy-Robertson, A.L., Peng, Y., 2011. Comparison of different vegetation indices for the remote assessment of green leaf area index of crops. Remote Sens. Environ. 115, 3468–3478.
Wendlandt, W.W.M., Hecht, H.G., 1966. Reflectance Spectroscopy. John Wiley & Sons (Interscience Publishers), New York, NY.
Wu, C., Niu, Z., Tang, Q., Huang, W., Rivard, B., Feng, J., 2009. Remote estimation of gross primary production in wheat using chlorophyll-related vegetation indices. Agric. For. Meteorol. 149, 1015–1021.
Xia, J., Niu, S., Ciais, P., Janssens, I.A., Chen, J., Ammann, C., Arain, A., Blanken, P.D., Cescatti, A., Bonal, D., 2015. Joint control of terrestrial gross primary productivity by plant phenology and physiology. Proc. Natl. Acad. Sci. 112, 2788–2793.
Yang, L., Kruse, B., 2004. Revised Kubelka–Munk theory. I. Theory and application. J. Opt. Soc. Am. A 21, 1933–1941.
Youngentob, K.N., Yoon, H.J., Stein, J., Lindenmayer, D.B., Held, A.A., 2015. Where the wild things are: using remotely sensed forest productivity to assess arboreal marsupial species richness and abundance. Divers. Distrib. 21, 977–990.
Yu, K., Lenz-Wiedemann, V., Chen, X., Bareth, G., 2014. Estimating leaf chlorophyll of barley at different growth stages using spectral indices to reduce soil background and canopy structure effects. ISPRS J. Photogramm. Remote Sens. 97, 58–77.
Zou, X., Hernández-Clemente, R., Tammeorg, P., Lizarazo Torres, C., Stoddard, F.L., Mäkelä, P., Pellikka, P., Mõttus, M., 2015. Retrieval of leaf chlorophyll content in field crops using narrow-band indices: effects of leaf area index and leaf mean tilt angle. Int. J. Remote Sens. 36, 6031–6055.